Anisotropic Third-Order Nonlinearity in Pristine and Lithium Hydride Intercalated Black Phosphorus

Tieshan Yang,[†] Ibrahim Abdelwahab,[‡,§] Han Lin,[†] Yang Bao,[‡] Sherman Jun Rong Tan,[‡,§]
Scott Fraser,[†] Kian Ping Loh,*[,‡,∥] and Baohua Jia*[,†]

[†]Centre for Micro-Photonics, Faculty of Science, Engineering and Technology, Swinburne University of Technology, Hawthorn, Victoria 3122, Australia

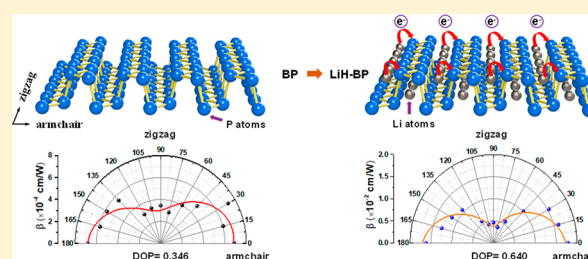[‡]Department of Chemistry, National University of Singapore, Singapore 117543, Singapore

[§]NUS Graduate School for Integrative Sciences and Engineering, Centre for Life Sciences, National University of Singapore, #05-01, 28 Medical Drive, Singapore 117456, Singapore

[∥]Centre for Advanced 2D Materials and Graphene Research Centre, National University of Singapore, Singapore 117546, Singapore

S *Supporting Information*

ABSTRACT: Two-dimensional (2D) black phosphorus (BP) displays unique anisotropic properties in its linear optical responses, but its third-order nonlinearity (Kerr effect) has remained relatively unexplored. Here we measured the third-order nonlinear optical responses in exfoliated BP and in lithium hydride intercalated BP (LiH-BP) flakes using polarization-resolved microscopic femtosecond Z-scan techniques. Strong optical Kerr nonlinearities were measured for single flakes of BP and LiH-BP, with third-order nonlinear susceptibilities that are larger than those for many 2D materials. The nonlinear coefficients of LiH-BP are higher than those of BP, indicating that lithium hydride intercalation enhances not only the ambient stability of BP but also its nonlinear optical response. Highly anisotropic polarization-dependent Kerr nonlinearities of both BP and LiH-BP flakes were observed. The strong nonlinear and anisotropic optical responses of BP and LiH-BP indicate the great potential of these materials in nonlinear photonics device applications.

KEYWORDS: *black phosphorus, lithium hydride intercalated black phosphorus, in-plane anisotropy, nonlinear optical responses, Kerr nonlinearity*

Black phosphorus (BP), a layered crystal consisting of only phosphorus atoms, has attracted renewed attention due to its semiconducting nature and layer-dependent direct band gap that can be tuned over a wide range (0.3 eV for the bulk to 2.0 eV for a monolayer), thus bridging the gap between zero-band-gap graphene and large-band-gap transition-metal dichalcogenides (TMDCs).[1−9] BP is a promising material for broad near- and mid-infrared photonics and optoelectronics applications, such as transistors, lasers, and photodetectors.[5,10−15] However, the rapid degradation of BP under ambient conditions limits its practical applications. Several approaches to passivate the surface and stabilize BP have been reported recently, which include coating Al_2O_3 using atomic layer deposition,[16,17] encapsulation by hexagonal boron nitride (*h*-BN),[18,19] oxygen plasma etching followed by Al_2O_3 coating,[20] and covalent functionalization.[21] These procedures have been found to introduce irreversible and undesirable defects and modifications to BP, resulting in degraded device performance. In this context, Sherman et al. recently reported alkali-metal-intercalated air-stable BP that was suitable for electronic and optoelectronic applications,[22] where lithium was intercalated into BP under ultrahigh vacuum (UHV) followed by in situ

hydrogenation (abbreviated as LiH-BP); this approach effectively solved the stability in BP.

The puckered nature of BP gives rise to optical and electronic anisotropy, which is manifested strongly along the armchair and zigzag directions.[6,23] Linear optical responses including optical spectrum (transmission, reflection, and absorption), Raman scattering, photoluminescence (PL), and photoresponsivity are polarization dependent.[23−31] Third-harmonic generation (THG) has been demonstrated in multilayer BP flakes, where both polarization and thickness dependence were noted.[32−34] However, the optical Kerr effect, which is crucial for optical switching, single regeneration, and optical communication in high-performance integrated photonics devices, has not been characterized in BP.[35,36] Previous experimental investigations on the Kerr nonlinearity in BP have been performed using solutions of BP flakes or in the form of composites containing randomly oriented/distributed flakes. For example, saturable absorption was observed in BP solutions using Z-scan techniques.[11,31,37−39] Lu et al. reported
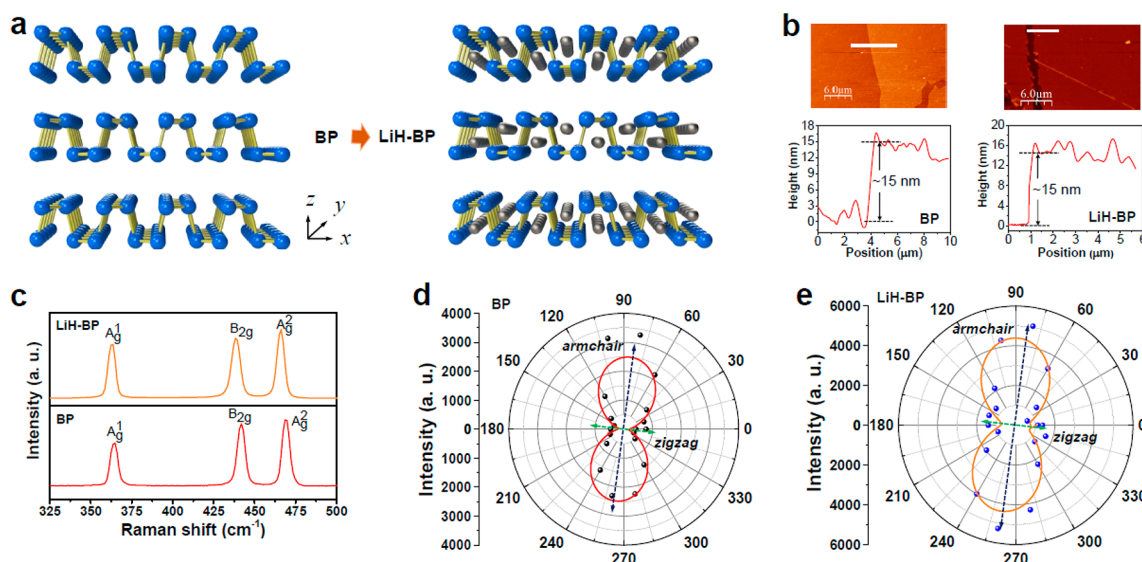
Figure 1. (a) Schematic of the crystal structure of black phosphorus (BP, left) and lithium intercalated black phosphorus (LiH-BP, right). Silver balls represent lithium atoms. The x (armchair) and y (zigzag) axes are directed along and perpendicular to the atomic bulk of BP, respectively. (b) Representative AFM images and height profiles of BP and LiH-BP flakes. The height profiles across BP and LiH-BP flakes are marked by the white lines. (c) Raman spectra of BP and LiH-BP flakes. The laser excitation wavelength is 532 nm. Polarization-resolved Raman spectra of BP (d) and LiH-BP (e) with linearly polarized laser excitation.

that BP composites showed broad-band saturable absorption ranging from the visible (400 nm) up to the mid-infrared (~1930 nm),[11] and Zheng et al. observed saturable absorption and two-photon absorption (TPA) of BP nanoplatelets at 800 nm, where the nonlinear refractive index was measured using a closed-aperture Z-scan configuration.[39] Zhang et al. measured the size-dependent saturable absorption of dispersed BP nanosheets and applied it for fiber laser mode locking.[40] Common to all these works were the random orientation and nonuniform thickness of the BP flakes, leading to considerable variations in the reported nonlinearity. The nonlinear properties of a single-crystal BP flake, as well as its polarization dependence, have not been studied systematically so far.

Herein, the polarization-dependent nonlinear properties of single crystals of 2D materials were recorded using a customized microscopic Z-scan setup having both spatial- and polarization-resolving abilities. We used both single BP and air-stable LiH-BP flakes in our measurements to reveal polarization-dependent third-order nonlinearity in these two systems. We find that both BP and LiH-BP flakes have large nonlinear absorption coefficients (β) and nonlinear refractive indices (n_2), which are highly anisotropic and depend on the incident polarization. We further find that the nonlinear absorption coefficient and nonlinear refractive index of LiH-BP are both higher than those of BP, indicating that Li intercalation efficiently enhances the nonlinear optical responses of pristine BP. We have attributed this enhancement to the efficient photoinduced energy and charge (electron) transfer between the Li atoms (donor) and phosphorus atoms (acceptor).

■ RESULTS AND DISCUSSION

Figure 1a schematizes the atomic structures of BP and LiH-BP, where Li atoms are inserted into the trenches in the BP structure.[22] The representative atomic force microscopy (AFM) images and height profiles of BP and LiH-BP flakes

are presented in Figure 1b; both thicknesses are measured to be ~15 nm.

The puckered atomic corrugation in the crystal structure of BP flakes induces in-plane anisotropy that is not observed in 2D materials, such as graphene and TMDCs. This structural anisotropy causes the in-plane photon−matter and electron−matter interactions to be different along the armchair direction (x axis) and the zigzag direction (y axis) (see Figure 1a). Raman spectra of BP and LiH-BP flakes obtained by excitation with a laser of 532 nm wavelength along the z direction are shown in Figure 1c. The three Raman peaks of LiH-BP flakes are in accordance with the characteristic A_g^1, B_{2g}, and A_g^2 vibration modes of the BP crystal lattice. Raman scattering peaks showed no spectral shift when the input polarizations were changed along the two crystalline axes, but the spectral intensities changed dramatically. In BP, the atomic motion associated with the A_g^2 mode occurs primarily along the armchair direction, which means that the associated Raman scattering intensity is the strongest when the excitation laser polarization is aligned along the armchair direction. In our polarization-resolved Raman experiment, the excitation light is linearly polarized and the polarization analyzer is kept parallel to the direction of the polarization of the excitation beam. Thus, the intensity of the A_g^2 mode can be used to determine the crystal orientation of the flake by rotating the flakes and measuring the angular dependence of the Raman scattering intensity of the A_g^2 mode.[26] The measured angular dependences of the A_g^2 mode intensity for BP and LiH-BP flakes are shown in Figure 1d,e, respectively. A maximum intensity at ~80° is seen in Figure 1e, which can be identified as the armchair direction of the BP flake. Our results also clearly prove that the unique anisotropy of BP is retained after LiH intercalation (Figure 1e).

To determine the polarization-dependent linear absorption coefficient (α), which is essential for the calculation of the two-photon absorption coefficient β and the refractive index n_2, we characterized the linear absorption properties of BP and LiH-BP flakes using Fourier transform infrared (FTIR) spectros-
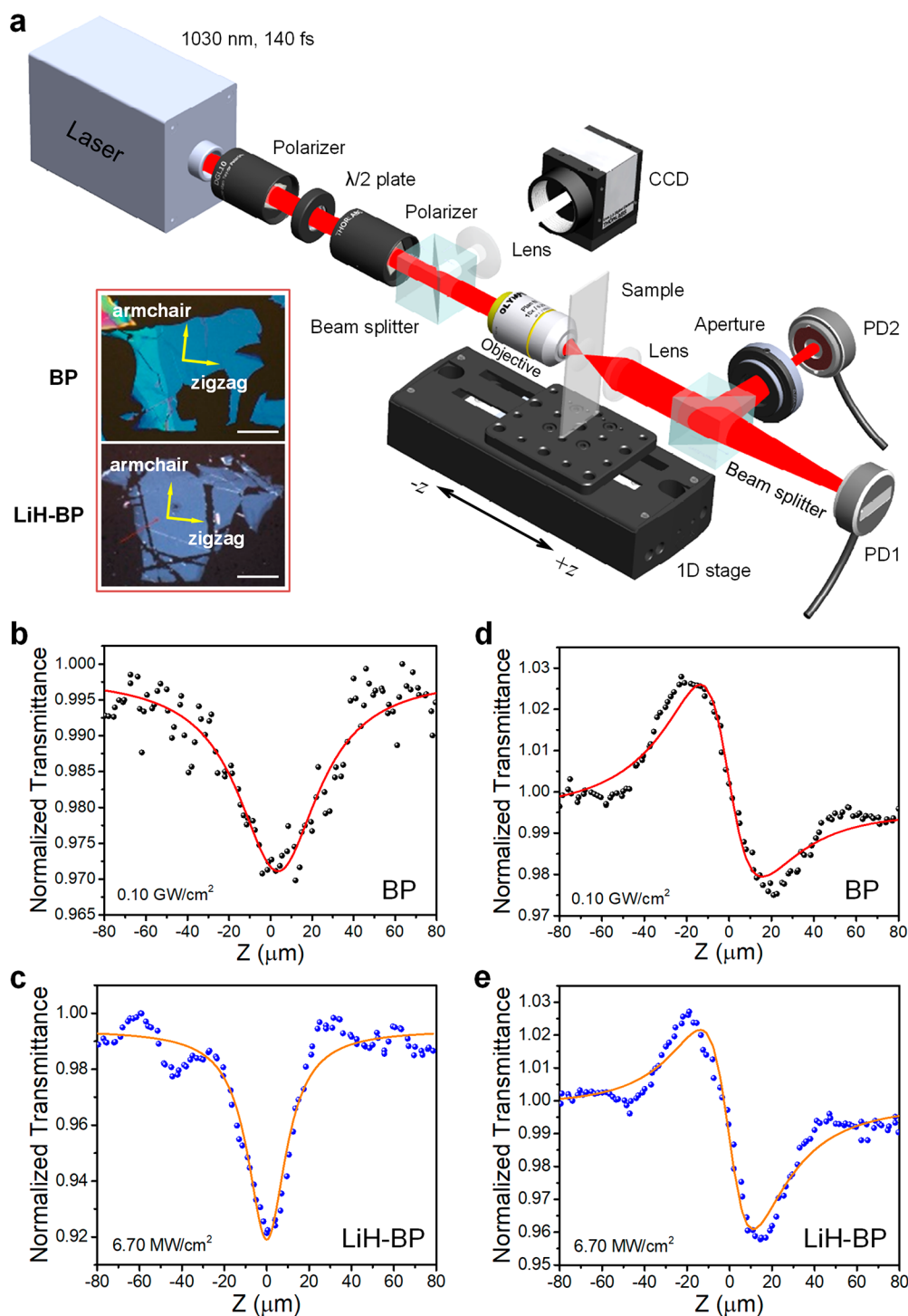
Figure 2. (a) Schematic diagram of the polarization-resolved microscopic Z-scan system used for the nonlinear absorption and refraction experiment. PD denotes the photodetector. Scale bar: 10 μm. Open-aperture (b, c) and closed-aperture (d, e) Z-scan traces of BP and LiH-BP flakes under femtosecond laser excitation at a wavelength of 1030 nm. Solid lines indicate theoretical fits to the measured data. (b) and (d) give the data for a BP flake, and (c) and (e) give the data for an LiH-BP flake.

copy (Section 2 in the Supporting Information). As expected, the direction of polarization of the incident light strongly affects the transmittance (or the absorption) of BP and LiH-BP flakes, which is consistent with results reported in the literature.[31] For example, the transmittance of the 15 nm BP flake at the wavelength of 1030 nm can increase from 77% to 99% when the input polarization direction is changed by 90°. Likewise, for the 15 nm LiH-BP flake, we observed that the

transmittance increased from 61% to 77% when the input polarization direction was altered by 90°. The polarization directions corresponding to the minimum and maximum transmittance are assigned to be the armchair and zigzag directions of the single flake.

As discussed above, it is necessary to measure the optical properties of single-crystal BP flakes to confirm polarization dependence, because flakes in nanocomposites or in solutions

Table 1. β and n_2 Values of Various 2D Materials Taken from the Literature

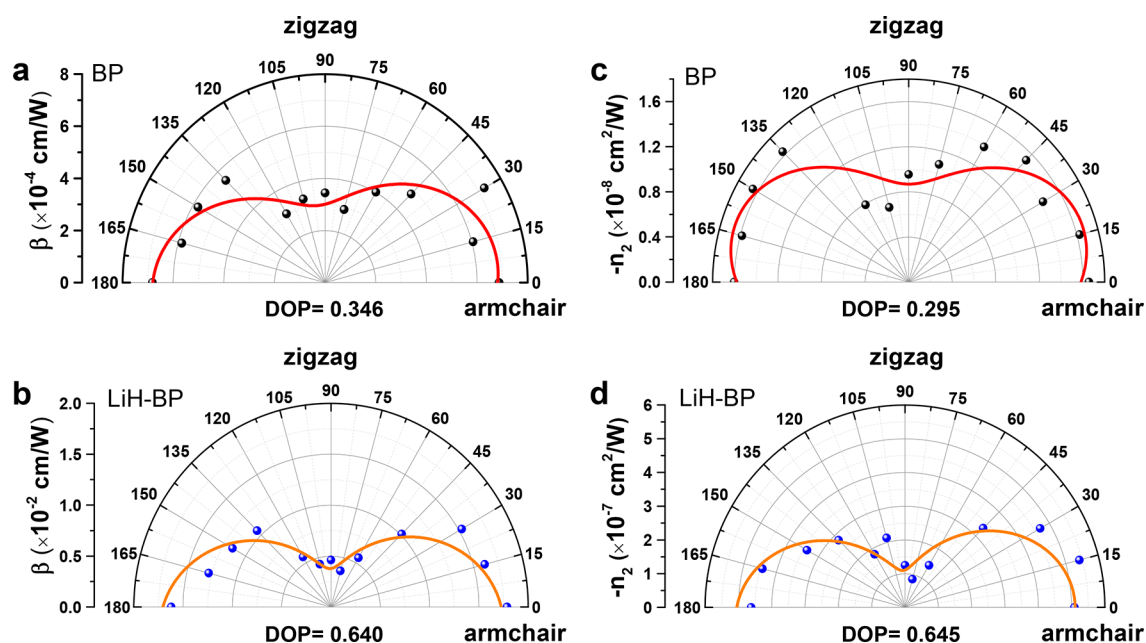| material	laser param	thickness (nm)	β (cm/W)	n_2 (cm^2/W)	ref
BP	1030 nm, 140 fs	15	5.845×10^{-4}	-1.635×10^{-8}	this work
LiH-BP	1030 nm, 140 fs	15	2.136×10^{-2}	-1.816×10^{-7}	this work
BP	800 nm, 100 fs	30−60	$(4.5 \pm 0.2) \times 10^{-8}$	$(6.8 \pm 0.2) \times 10^{-9}$	39
MoS$_2$	1030 nm, 340 fs	18−19.44	$(66 \pm 4) \times 10^{-9}$	N/A	43
WS$_2$	1040 nm, 340 fs	0.75	$(3.07 \pm 1.31) \times 10^{-6}$	$(1.28 \pm 0.03) \times 10^{-10}$	44
WSe$_2$	1040 nm, 340 fs	5.5	$(5.29 \pm 0.06) \times 10^{-6}$	N/A	44
graphene	1150 nm, 100 fs	5−7 layers	5.845×10^{-6}	$\sim 10^{-9}$	45

Figure 3. Anisotropic nonlinear optical responses of BP and LiH-BP flakes of 15 nm thickness. Dependence of nonlinear absorption coefficient of BP (a) and LiH-BP (b) on the incident polarization. Dependence of nonlinear refractive index of BP (c) and LiH-BP (d) on the incident polarization. 0 and 90° correspond to the armchair and zigzag directions, respectively. The lines in the polar plots are cosine-squared fits of the experimental data (dots). The calculated DOP values are shown at the bottom of each polar plot.

have random orientations that average out polarization effects. However, a conventional Z-scan setup with low-resolution lenses cannot be used to measure individual flakes, due to the large size of the focal spot, as a result of which multiple flakes with random orientations are illuminated and crystal orientations cannot be identified. To address this challenge, we constructed a microscopic Z-scan setup with polarization selectivity capable of focusing light onto a particular selected single crystal of BP or LiH-BP (see Figure 2a, Methods, and Section 3 in the Supporting Information for details). A CCD camera was introduced to visualize the flakes and the focal spot, which allowed us to control the polarization of the incident light relative to the crystal orientations of the BP and LiH-BP flakes with high precision down to 1°. The Kerr nonlinear optical responses of the BP and LiH-BP flakes were measured by using a femtosecond laser with a central wavelength of 1030 nm and a pulse duration of 140 fs (Section 3 in the Supporting Information), as shown in Figure 2a. To accurately focus the beam on the targeted flakes, an objective lens (magnification 10×, numerical aperture 0.25) combined with a CCD camera was used to directly observe the transmitted laser beam. The microscopic images of the single-crystal BP and LiH-BP flakes are shown in the insets of Figure 2a.

The open- and closed-aperture Z-scan results of 15 nm thickness BP and LiH-BP flakes are presented in Figures 2b−e. As shown in Figure 2b, even at a very low laser intensity of 0.10 GW/cm^2, two-photon absorption (TPA) can be observed from the BP flake. The extracted nonlinear absorption coefficient, β, is 5.845×10^{-4} cm/W, which is 4 orders of magnitude higher than previously reported values for BP in solution or in a composite. One explanation is our Z-scan measurement directly measures individual crystal flakes visualized using the CCD camera and does not average over sparsely distributed flakes of various thicknesses and with different orientations. The TPA process is characteristic of photoexcited excitonic absorption, and it is likely that this large TPA coefficient originates from a strong excitonic effect.[41,42]

Remarkably, the LiH-BP flake exhibits TPA at an even lower input laser intensity of 6.70 MW/cm^2 (Figure 2c), which is 2 orders of magnitude smaller than that required for a pristine BP flake. This yields a nonlinear absorption coefficient β of 2.136×10^{-2} cm/W for LiH-BP, which is 2 orders of magnitude larger than that of pristine BP. One explanation is that photoinduced energy and charge (electron) transfer under laser illumination may result in strong donor (Li atoms)−acceptor (P atoms) interactions, boosting exciton−photon coupling and leading to the enhancement of nonlinear absorption.
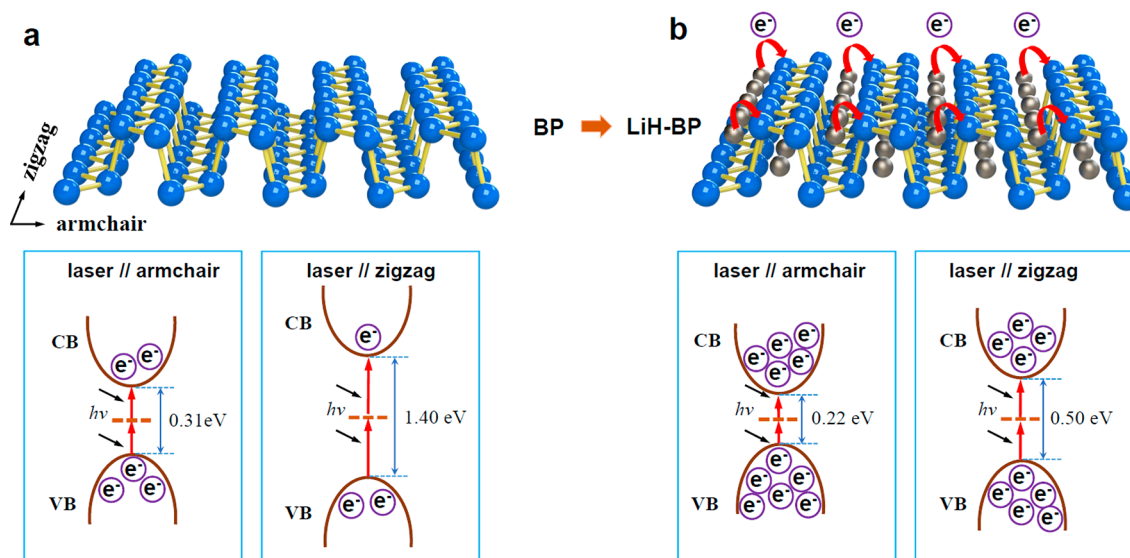
Figure 4. Schematic illustration of the polarization-dependent TPA of BP (a) and LiH-BP (b) flakes. The band gap and defect energy levels were determined from high-resolution electron energy loss spectroscopy (HREELS) measurements, combined with the relationship between the absorption coefficient and incident photon energy. CB denotes the conduction band and VB the valence band.

In addition, closed-aperture Z-scan results shown in Figure 2d reveal a strong optical Kerr nonlinearity for the BP flake, as evidenced from the pronounced peak−valley curve, typical of a self-defocusing effect. The derived nonlinear refractive index, n_2, is -1.635×10^{-8} cm^2/W at an input laser intensity of 0.10 GW/cm^2. Similar to pristine BP, the LiH-BP flake also exhibits a peak−valley curve at an input laser intensity of 6.70 MW/cm^2, as shown in Figure 2e, which yields a nonlinear refractive index n_2 of -1.816×10^{-7} cm^2/W that is 1 order of magnitude larger than that of pristine BP. The strong optical Kerr nonlinearity discovered in single-crystal BP and LiH-BP flakes is higher than that observed for most other 2D materials (Table 1), indicating that pristine BP and air-stable LiH-BP flakes have great potential as candidate materials for nonlinear microscopic imaging and optical signal modulation in optoelectronic platforms. It is clear from the open- and closed-aperture Z-scan results that lithium hydride intercalation significantly enhances the nonlinear optical properties of BP flakes.

Using a polarization-resolved Z-scan setup, we studied the anisotropic nonlinear optical responses of individual BP and LiH-BP flakes. In our microscopic Z-scan setup, we have combined a half-wave plate (HWP) and a linear polarizer to control the laser polarization angle and to attenuate the incident laser power. The polar plots of β and n_2 for both BP and LiH-BP flakes as a function of the incident polarization angle are shown in Figure 3. A clear polarization-dependent third-order nonlinearity is observed. The nonlinearity is higher in the armchair direction, which is consistent with the observed linear properties.

To quantify the polarization-dependent nonlinearity, we define a parameter called the degree of polarization (DOP) according to

$$\text{DOP} = \frac{A_{\max} - A_{\min}}{A_{\max} + A_{\min}} \tag{1}$$

where $A_{\max}$ and $A_{\min}$ are the maximum and minimum values in the polar plot, respectively (for example, totally polarized light

has a DOP value of 1, whereas unpolarized light has a DOP value of 0).

As shown in Figure 3, the DOP values of β and n_2 are 0.346 and 0.295, respectively, for the BP flake. Due to the birefringence of the BP flakes, the nonlinear optical responses can be decomposed into two components along the armchair and zigzag directions of a BP crystal. A maximum in the nonlinear optical response corresponds to an incident polarization aligned along the armchair direction of the flakes.

In comparison, the DOP values of β and n_2 for the LiH-BP flake are 0.640 and 0.645, respectively, which are significantly higher than those for pristine BP flakes, indicating that lithium intercalation not only stabilizes a BP flake but also enhances its anisotropic nonlinear optical responses. This is important for the application of BP in nonlinear photonics devices requiring a stable performance at high excitation intensity.

The amplitude of the third-order nonlinear polarization is given by $P^{(3)}(\omega) = \frac{3\varepsilon_0}{4}\chi_{\text{eff}}^{(3)}E^3$,[46] where ε_0 is the dielectric permittivity and $\chi_{\text{eff}}^{(3)}$ is the effective third-order susceptibility, whose functional form depends on the symmetry and orientation of the crystal. The intensity-dependent TPA coefficient β and n_2 are related respectively to the imaginary and real part of $\chi^{(3)}$ by[47]

$$\beta \text{ (m/W)} = \frac{3\omega}{2\varepsilon_0 c^2 n_0^2} Im\chi^{(3)}(\omega; -\omega, \omega, \omega) \tag{2}$$

$$n_2 \text{ (m}^2\text{/W)} = \frac{3}{4\varepsilon_0 c n_0^2} Re\chi^{(3)}(\omega; -\omega, \omega, \omega) \tag{3}$$

where n_0 is the linear refractive index and c is the speed of light in a vacuum.

The spatial symmetry of BP restricts the form of the effective third-order susceptibility tensor, which in turn determines its nonlinear optical responses for the different polarization states of the incident beam. BP has a puckered orthorhombic crystal structure belonging to the D_{2h} point group.[32] The effective third-order susceptibility tensor associated with BP has 21 independent nonzero elements: 3 elements with all equal indices and 18 coefficients with indices equal in pairs. For a
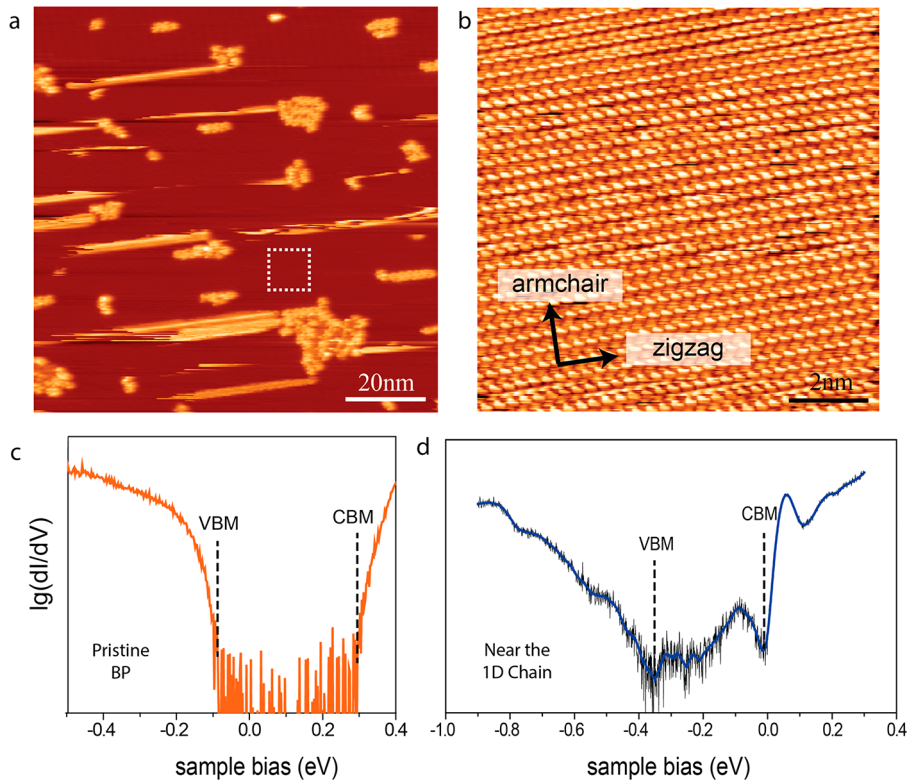
Figure 5. (a) STM image of the K-covered BP surface, showing 1D chains and 2D clusters of self-assembled K atoms. (b) STM image of the clean BP surface, indicated by the white dashed box in (a). (c) dI/dV spectrum collected on pristine BP before K deposition. (d) dI/dV spectrum taken on a clean BP surface near the 1D K atomic chains. CBM denotes the conduction band minimum and VBM the valence band maximum.

linearly polarized incident beam propagating along the z direction, the electric field is in the xy plane at an angle φ to the x axis (armchair direction of BP flakes); the electric field can be expressed according to $\vec{E} = E_0(\cos\varphi\vec{x} + \sin\varphi\vec{y})$. Thus, the effective third-order susceptibility is[46,48]

$$\chi_{\text{eff}}^{(3)}(\varphi) = \chi_{xxxx}^{(3)}\cos^4\varphi + \chi_{yyyy}^{(3)}\sin^4\varphi + B\frac{\sin^2 2\varphi}{4} \quad (4)$$

$$B = 2\chi_{xxyy}^{(3)} + 2\chi_{yyxx}^{(3)} + \chi_{xyyx}^{(3)} + \chi_{yxxy}^{(3)} \quad (5)$$

Figure 3 shows plots of the nonlinear coefficients β and n_2 of BP and LiH-BP flakes as a function of the polarization orientation angle φ. The observed oscillations of both β and n_2 with respect to the incident polarization angle clearly points to the in-plane polarization dependence of the third-order nonlinearity in BP and LiH-BP flakes.

To gain a further understanding of the polarization-dependent nonlinearity, we discuss the measured TPA coefficients of our BP and LiH-BP single flakes in terms of a simple two-band model by directly taking the band dispersion into account, as shown in Figure 4. The TPA based on the two-band model is described by[49,50]

$$\beta(\lambda, E_g) = K\frac{\sqrt{E_0}}{n_0^2 E_g^3}F_2(x) \quad (6)$$

where the Kane parameter (K) and E_0 (~21 eV for typical direct-band-gap semiconductors) are constants, n_0 is the refractive index, $x = \hbar\omega/E_g = hc/\lambda E_g$ is the dispersion parameter, E_g is the band gap, and $F_2(x)$ is the universal β

dispersion function. Considering two parabolic bands for near-band-edge optical transitions, $F_2(x)$ is given by[49,50]

$$F_2(x) = \frac{(2x-1)^{3/2}}{(2x)^5} \quad (7)$$

Hence,

$$\beta(\lambda, E_g) = K\frac{\sqrt{E_0}}{n_0^2}\frac{\lambda^{7/2}(2hc - \lambda E_g)^{3/2}E_g^{1/2}}{(2hc)^5} \quad (8)$$

From eq 8, we can see that β increases as E_g decreases. From the polarization-dependent linear absorption (Figure S2 in the Supporting Information), we can see that the bandgaps are different along the zigzag and armchair directions. The band gap of BP flakes was measured by high-resolution electron energy loss spectroscopy (HREELS, Section 4 in the Supporting Information). The azimuth of the sample holder is rotated along the armchair direction of the BP flake, and the band gap is determined to be 0.31 eV (Figure S4 in the Supporting Information). We are able to calculate the band gaps of the BP flake along the zigzag direction, which is 1.4 eV, on the basis of the relationship between the absorption coefficient and incident photon energy (Section 4 in the Supporting Information). This result in combination with eq 8 confirms the polarization-dependent TPA in a BP flake (Figure 4a). In a similar manner, the calculated band gaps of LiH-BP along the armchair and zigzag directions are 0.22 and 0.50 eV, respectively (Section 4 in the Supporting Information). Thus, according to eq 8, we see that a corresponding increase in TPA along both the armchair and zigzag directions is expected, which is confirmed by the experimental results (Figure 4b).

4974

The distribution of the alkali metal in BP trenches is experimentally verified from low-temperature scanning tunneling microscopy (STM) experiments. As Li atoms are too mobile to be imaged by STM, we have chosen K atoms, since the interaction of K with BP should be similar to that of Li. The STM image in Figure 5a clearly shows that, following in situ deposition of K, the BP surface is partially covered by one-dimensional (1D) chains of self-assembled K atoms along the zigzag trenches on the BP surface (Figure 5b). The strongly anisotropic spatial distribution of K atoms accounts for the much stronger anisotropic nonlinear optical response of LiH-BP in comparison to pristine BP. The 1D distribution of alkali metals along the zigzag direction also accentuates the difference in electronic properties between armchair and zigzag directions. The typical dI/dV spectrum of pristine BP shows a band gap of ∼0.3 eV, and the Fermi level (simple bias 0 V) is close to the valence band edge, indicating that pristine BP is slightly p doped (Figure 5c), which is consistent with previous reports.[51] The dI/dV spectra collected in the vicinity of the 1D K atom chains reveal that the Fermi level is shifted toward the conduction band edge, suggesting that the BP lattice near the K atom is heavily n doped (Figure 5d). The intercalated LiH donates electrons to BP, and this donor–acceptor interaction creates a dipole and leads to enhanced nonlinear optical properties.[36]

CONCLUSION

Using a custom-designed polarization-resolved microscopic femtosecond Z-scan setup, we observed strong third-order nonlinear optical responses in single-crystal BP and LiH-BP flakes. The nonlinear absorption coefficient and nonlinear refractive index of LiH-BP are both higher than those of BP, demonstrating that lithium hydride intercalation enhances the nonlinear optical response due to donor–acceptor type interactions. The LiH-BP flake presents significantly higher anisotropy in third-order nonlinearity. The band gap difference, efficient energy, and charge (electron) transfer upon photoexcitation and the synergistic coupling effects between the Li and P atoms play an important role in enhancing the optical nonlinearity. The strong nonlinear and anisotropic optical responses of BP and LiH-BP are expected to be important for their application in mid-infrared nonlinear photonics devices.

METHODS

Sample Preparation. Ultrathin BP nanosheets were mechanically exfoliated from bulk crystals (HQgraphene) onto quartz substrates using a Scotch tape method in an argon-filled glovebox. Some of the substrates were transferred using a vacuum transfer box to an ultrahigh-vacuum chamber for Li intercalation, which was performed by evaporating Li atoms form a standard SAES (Società Apparecchi Electrici Scientifici) getter source at a rate of 0.3 monolayer/hour (Section 1 in the Supporting Information). Angle-resolved X-ray photoelectron spectroscopy (XPS) measurement on the Li-intercalated BP confirmed that Li was successfully intercalated in BP by in situ hydrogenation (Section 1 in the Supporting Information). The intercalated lithium was converted to lithium hydride (LiH) by heating the sample at 450 K in a hydrogen background pressure of 2×10^{-5} Torr. The Li to P ratio was determined to be 1:10, by integrating the area under Li 1s and P 2p core level peaks fitted with a mixed Gaussian–

Lorentzian line shape with a Shirley background subtraction. As we have documented previously, the LiH-intercalated BP is more stable inan ambient environment in comparison to the Li-intercalated sample or a pristine BP sample.[22] A thin layer of PMMA (∼100 nm) was spin-coated on the pristine BP samples before they were taken out of the glovebox for charaterization. BP and LiH-BP flakes of comparable thicknesses (∼15 nm) were selected for the nonlinear optical measurements, and the thickness of the flakes was verified using atomic force microscopy (AFM).

Optical Characterization. The linear optical properties of BP and LiH-BP were investigated by polarization-resolved Raman spectroscopy (WITec alpha 300R) and Fourier transform infrared (FTIR) spectroscopy (Bruker Hyperion 2000). The nonlinear optical properties of BP and LiH-BP nanosheets were measured by a Z-scan setup equipped with a femtosecond laser (Coherent, Chameleon) with a central wavelength of 1030 nm and a pulse duration of 140 fs (Section 3 in the Supporting Information), as shown in Figure 2a. In our Z-scan setup, a CCD camera was introduced to visualize the flakes and the focal spot, which allowed us to control the polarization of the incident light relative to the crystal orientations of the BP and LiH-BP flakes with high precision down to 1°. To accurately focus the beam on the targeted flakes, an objective lens (magnification 10×, numerical aperture 0.25) combined with a CCD camera was used to directly observe the transmitted laser beam.

ASSOCIATED CONTENT

Ⓢ Supporting Information

The Supporting Information is available free of charge on the ACS Publications website at DOI: 10.1021/acsphotonics.8b01200.

> Angle-resolved XPS, polarization dependent FTIR, polarization-resolved microscopic Z-scan method, and high-resolution electron energy loss spectroscopy (HREELS) measurements (PDF)

AUTHOR INFORMATION

Corresponding Authors
*E-mail for K.P.L.: chmlohkp@nus.edu.sg.
*E-mail for B.J.: bjia@swin.edu.au.
ORCID
Ibrahim Abdelwahab: 0000-0002-0107-5827
Sherman Jun Rong Tan: 0000-0003-1591-3497
Kian Ping Loh: 0000-0002-1491-743X
Baohua Jia: 0000-0002-6703-477X
Notes
The authors declare no competing financial interest.

ACKNOWLEDGMENTS

REFERENCES

(1) Novoselov, K. S.; Geim, A. K.; Morozov, S. V.; Jiang, D.; Zhang, Y.; Dubonos, S. V.; Grigorieva, I. V.; Firsov, A. A. Electric Field Effect in Atomically Thin Carbon Films. *Science* **2004**, *306*, 666−669.

(2) Bonaccorso, F.; Sun, Z.; Hasan, T.; Ferrari, A. Graphene photonics and optoelectronics. *Nat. Photonics* **2010**, *4*, 611−622.

(3) Bhimanapati, G. R.; Lin, Z.; Meunier, V.; Jung, Y.; Cha, J.; Das, S.; Xiao, D.; Son, Y.; Strano, M. S.; Cooper, V. R.; Liang, L.; Louie, S. G.; Ringe, E.; Zhou, W.; Kim, S. S.; Naik, R. R.; Sumpter, B. G.; Terrones, H.; Xia, F.; Wang, Y.; Zhu, J.; Akinwande, D.; Alem, N.; Schuller, J. A.; Schaak, R. E.; Terrones, M.; Robinson, J. A. Recent Advances in Two-Dimensional Materials beyond Graphene. *ACS Nano* **2015**, *9*, 11509−11539.

(4) Mak, K. F.; Shan, J. Photonics and optoelectronics of 2D semiconductor transition metal dichalcogenides. *Nat. Photonics* **2016**, *10*, 216−226.

(5) Li, L.; Yu, Y.; Ye, G. J.; Ge, Q.; Ou, X.; Wu, H.; Feng, D.; Chen, X. H.; Zhang, Y. Black phosphorus field-effect transistors. *Nat. Nanotechnol.* **2014**, *9*, 372−377.

(6) Castellanos-Gomez, A. Black Phosphorus: Narrow Gap, Wide Applications. *J. Phys. Chem. Lett.* **2015**, *6*, 4280−91.

(7) Ling, X.; Wang, H.; Huang, S.; Xia, F.; Dresselhaus, M. S. The renaissance of black phosphorus. *Proc. Natl. Acad. Sci. U. S. A.* **2015**, *112*, 4523−30.

(8) Zhang, H. Ultrathin Two-Dimensional Nanomaterials. *ACS Nano* **2015**, *9*, 9451−9469.

(9) Liu, Y.; Rodrigues, J. N. B.; Luo, Y. Z.; Li, L.; Carvalho, A.; Yang, M.; Laksono, E.; Lu, J.; Bao, Y.; Xu, H.; Tan, S. J. R.; Qiu, Z.; Sow, C. H.; Feng, Y. P.; Neto, A. H. C.; Adam, S.; Lu, J.; Loh, K. P. Tailoring sample-wide pseudo-magnetic fields on a graphene-black phosphorus heterostructure. *Nat. Nanotechnol.* **2018**, *13*, 828−834.

(10) Du, H.; Lin, X.; Xu, Z.; Chu, D. Recent developments in black phosphorus transistors. *J. Mater. Chem. C* **2015**, *3*, 8760−8775.

(11) Lu, S. B.; Miao, L. L.; Guo, Z. N.; Qi, X.; Zhao, C. J.; Zhang, H.; Wen, S. C.; Tang, D. Y.; Fan, D. Y. Broadband nonlinear optical response in multi-layer black phosphorus: an emerging infrared and mid-infrared optical material. *Opt. Express* **2015**, *23*, 11183−94.

(12) Guo, Q.; Pospischil, A.; Bhuiyan, M.; Jiang, H.; Tian, H.; Farmer, D.; Deng, B.; Li, C.; Han, S.-J.; Wang, H.; Xia, Q.; Ma, T.-P.; Mueller, T.; Xia, F. Black Phosphorus Mid-Infrared Photodetectors with High Gain. *Nano Lett.* **2016**, *16*, 4648−4655.

(13) Zhao, Y.; Chen, Y.; Zhang, Y.-H.; Liu, S.-F. Recent advance in black phosphorus: Properties and applications. *Mater. Chem. Phys.* **2017**, *189*, 215−229.

(14) Wang, X.; Lan, S. Optical properties of black phosphorus. *Adv. Opt. Photonics* **2016**, *8*, 618.

(15) Yuan, H.; Liu, X.; Afshinmanesh, F.; Li, W.; Xu, G.; Sun, J.; Lian, B.; Curto, A. G.; Ye, G.; Hikita, Y.; Shen, Z.; Zhang, S.-C.; Chen, X.; Brongersma, M.; Hwang, H. Y.; Cui, Y. Polarization-sensitive broadband photodetector using a black phosphorus vertical p−n junction. *Nat. Nanotechnol.* **2015**, *10*, 707−713.

(16) Kim, J.-S.; Liu, Y.; Zhu, W.; Kim, S.; Wu, D.; Tao, L.; Dodabalapur, A.; Lai, K.; Akinwande, D. Toward air-stable multilayer phosphorene thin-films and transistors. *Sci. Rep.* **2015**, *5*, 8989.

(17) Na, J.; Lee, Y. T.; Lim, J. A.; Hwang, D. K.; Kim, G.-T.; Choi, W. K.; Song, Y.-W. Few-Layer Black Phosphorus Field-Effect Transistors with Reduced Current Fluctuation. *ACS Nano* **2014**, *8*, 11753−11762.

(18) Chen, X.; Wu, Y.; Wu, Z.; Han, Y.; Xu, S.; Wang, L.; Ye, W.; Han, T.; He, Y.; Cai, Y.; Wang, N. High-quality sandwiched black phosphorus heterostructure and its quantum oscillations. *Nat. Commun.* **2015**, *6*, 7315.

(19) Avsar, A.; Vera-Marun, I. J.; Tan, J. Y.; Watanabe, K.; Taniguchi, T.; Castro Neto, A. H.; Özyilmaz, B. Air-Stable Transport in Graphene-Contacted, Fully Encapsulated Ultrathin Black Phosphorus-Based Field-Effect Transistors. *ACS Nano* **2015**, *9*, 4138−4145.

(20) Pei, J.; Gai, X.; Yang, J.; Wang, X.; Yu, Z.; Choi, D.-Y.; Luther-Davies, B.; Lu, Y. Producing air-stable monolayers of phosphorene and their defect engineering. *Nat. Commun.* **2016**, *7*, 10450.

(21) Ryder, C. R.; Wood, J. D.; Wells, S. A.; Yang, Y.; Jariwala, D.; Marks, T. J.; Schatz, G. C.; Hersam, M. C. Covalent functionalization and passivation of exfoliated black phosphorus via aryl diazonium chemistry. *Nat. Chem.* **2016**, *8*, 597.

(22) Tan, S. J. R.; Abdelwahab, I.; Chu, L.; Poh, S. M.; Liu, Y.; Lu, J.; Chen, W.; Loh, K. P. Quasi-Monolayer Black Phosphorus with High Mobility and Air Stability. *Adv. Mater.* **2018**, *30*, 1704619.

(23) Xia, F.; Wang, H.; Jia, Y. Rediscovering black phosphorus as an anisotropic layered material for optoelectronics and electronics. *Nat. Commun.* **2014**, *5*, 4458.

(24) Wang, X.; Jones, A. M.; Seyler, K. L.; Tran, V.; Jia, Y.; Zhao, H.; Wang, H.; Yang, L.; Xu, X.; Xia, F. Highly anisotropic and robust excitons in monolayer black phosphorus. *Nat. Nanotechnol.* **2015**, *10*, 517−21.

(25) Kim, J.; Lee, J.-U.; Lee, J.; Park, H. J.; Lee, Z.; Lee, C.; Cheong, H. Anomalous polarization dependence of Raman scattering and crystallographic orientation of black phosphorus. *Nanoscale* **2015**, *7*, 18708−18715.

(26) Liu, S.; Huo, N.; Gan, S.; Li, Y.; Wei, Z.; Huang, B.; Liu, J.; Li, J.; Chen, H. Thickness-dependent Raman spectra, transport properties and infrared photoresponse of few-layer black phosphorus. *J. Mater. Chem. C* **2015**, *3*, 10974−10980.

(27) Ribeiro, H. B.; Pimenta, M. A.; de Matos, C. J. S.; Moreira, R. L.; Rodin, A. S.; Zapata, J. D.; de Souza, E. A. T.; Castro Neto, A. H. Unusual Angular Dependence of the Raman Response in Black Phosphorus. *ACS Nano* **2015**, *9*, 4270−4276.

(28) Wu, J.; Mao, N.; Xie, L.; Xu, H.; Zhang, J. Identifying the Crystalline Orientation of Black Phosphorus Using Angle-Resolved Polarized Raman Spectroscopy. *Angew. Chem.* **2015**, *127*, 2396−2399.

(29) Lan, S.; Rodrigues, S.; Kang, L.; Cai, W. Visualizing Optical Phase Anisotropy in Black Phosphorus. *ACS Photonics* **2016**, *3*, 1176−1181.

(30) Mao, N.; Tang, J.; Xie, L.; Wu, J.; Han, B.; Lin, J.; Deng, S.; Ji, W.; Xu, H.; Liu, K.; Tong, L.; Zhang, J. Optical Anisotropy of Black Phosphorus in the Visible Regime. *J. Am. Chem. Soc.* **2016**, *138*, 300−305.

(31) Li, D.; Jussila, H.; Karvonen, L.; Ye, G.; Lipsanen, H.; Chen, X.; Sun, Z. Polarization and Thickness Dependent Absorption Properties of Black Phosphorus: New Saturable Absorber for Ultrafast Pulse Generation. *Sci. Rep.* **2015**, *5*, 15899.

(32) Wu, H.-Y.; Yen, Y.; Liu, C.-H. Observation of polarization and thickness dependent third-harmonic generation in multilayer black phosphorus. *Appl. Phys. Lett.* **2016**, *109*, 261902.

(33) Youngblood, N.; Peng, R.; Nemilentsau, A.; Low, T.; Li, M. Layer-Tunable Third-Harmonic Generation in Multilayer Black Phosphorus. *ACS Photonics* **2017**, *4*, 8−14.

(34) Hipolito, F.; Pedersen, T. G. Optical third harmonic generation in black phosphorus. *Phys. Rev. B: Condens. Matter Mater. Phys.* **2018**, *97*, 035431.

(35) Zheng, X.; Jia, B.; Chen, X.; Gu, M. In situ third-order non-linear responses during laser reduction of graphene oxide thin films towards on-chip non-linear photonic devices. *Adv. Mater.* **2014**, *26*, 2699−703.

(36) Fraser, S.; Zheng, X.; Qiu, L.; Li, D.; Jia, B. Enhanced optical nonlinearities of hybrid graphene oxide films functionalized with gold nanoparticles. *Appl. Phys. Lett.* **2015**, *107*, 031112.

(37) Wang, Y.; Huang, G.; Mu, H.; Lin, S.; Chen, J.; Xiao, S.; Bao, Q.; He, J. Ultrafast recovery time and broadband saturable absorption properties of black phosphorus suspension. *Appl. Phys. Lett.* **2015**, *107*, 091905.

(38) Sotor, J.; Sobon, G.; Macherzynski, W.; Paletko, P.; Abramski, K. M. Black phosphorus saturable absorber for ultrashort pulse generation. *Appl. Phys. Lett.* **2015**, *107*, 051108.

(39) Zheng, X.; Chen, R.; Shi, G.; Zhang, J.; Xu, Z.; Cheng, X.; Jiang, T. Characterization of nonlinear properties of black phosphorus nanoplatelets with femtosecond pulsed Z-scan measurements. *Opt. Lett.* **2015**, *40*, 3480−3483.

(40) Zhang, S.; Zhang, X.; Wang, H.; Chen, B.; Wu, K.; Wang, K.; Hanlon, D.; Coleman, J. N.; Chen, J.; Zhang, L.; Wang, J. Size-dependent saturable absorption and mode-locking of dispersed black phosphorus nanosheets. *Opt. Mater. Express* **2016**, *6*, 3159.

(41) Sheik-Bahae, M.; Hagan, D. J.; Van Stryland, E. W. Dispersion and band-gap scaling of the electronic Kerr effect in solids associated with two-photon absorption. *Phys. Rev. Lett.* **1990**, *65*, 96−99.

(42) Li, Y.; Dong, N.; Zhang, S.; Zhang, X.; Feng, Y.; Wang, K.; Zhang, L.; Wang, J. Giant two-photon absorption in monolayer MoS_2. *Laser Photonics Rev.* **2015**, *9*, 427−434.

(43) Zhang, S.; Dong, N.; McEvoy, N.; O'Brien, M.; Winters, S.; Berner, N. C.; Yim, C.; Li, Y.; Zhang, X.; Chen, Z.; Zhang, L.; Duesberg, G. S.; Wang, J. Direct Observation of Degenerate Two-Photon Absorption and Its Saturation in WS_2 and MoS_2 Monolayer and Few-Layer Films. *ACS Nano* **2015**, *9* (7), 7142−7150.

(44) Dong, N.; Li, Y.; Zhang, S.; McEvoy, N.; Zhang, X.; Cui, Y.; Zhang, L.; Duesberg, G. S.; Wang, J. Dispersion of nonlinear refractive index in layered WS_2 and WSe_2 semiconductor films induced by two-photon absorption. *Opt. Lett.* **2016**, *41*, 3936−3939.

(45) Demetriou, G.; Bookey, H. T.; Biancalana, F.; Abraham, E.; Wang, Y.; Ji, W.; Kar, A. K. Nonlinear optical properties of multilayer graphene in the infrared. *Opt. Express* **2016**, *24*, 13033−13043.

(46) DeSalvo, R.; Sheik-Bahae, M.; Said, A. A.; Hagan, D. J.; Van Stryland, E. W. Z-scan measurements of the anisotropy of nonlinear refraction and absorption in crystals. *Opt. Lett.* **1993**, *18*, 194−196.

(47) Sheik-Bahae, M.; Said, A. A.; Wei, T. H.; Hagan, D. J.; Stryland, E. W. V. Sensitive measurement of optical nonlinearities using a single beam. *IEEE J. Quantum Electron.* **1990**, *26*, 760−769.

(48) Fang, Y.; Zhou, F.; Yang, J.; Wu, X.; Xiao, Z.; Li, Z.; Song, Y. Anisotropy of two-photon absorption and free-carrier effect in nonpolar GaN. *Appl. Phys. Lett.* **2015**, *106*, 131903.

(49) Van Stryland, E. W.; Vanherzeele, H.; Woodall, M. A.; Soileau, M. J.; Smirl, A. L.; Guha, S.; Boggess, T. F. Two Photon Absorption, Nonlinear Refraction, And Optical Limiting In Semiconductors. *Opt. Eng.* **1985**, *24*, 244613.

(50) Saouma, F. O.; Park, D. Y.; Kim, S. H.; Jeong, M. S.; Jang, J. I. Multiphoton Absorption Coefficients of Organic-Inorganic Lead Halide Perovskites $CH_3NH_3PbX_3$ (X = Cl, Br, I) Single Crystals. *Chem. Mater.* **2017**, *29*, 6876−6882.

(51) Liu, Y.; Qiu, Z.; Carvalho, A.; Bao, Y.; Xu, H.; Tan, S. J. R.; Liu, W.; Castro Neto, A. H.; Loh, K. P.; Lu, J. Gate-Tunable Giant Stark Effect in Few-Layer Black Phosphorus. *Nano Lett.* **2017**, *17*, 1970−1977.